

GALAXIES INTO THE DARK AGES

C. L. CARILLI^{1,2}, E. J. MURPHY³, A. FERRARA^{4,5}, P. DAYAL⁶

Draft version October 8, 2018

ABSTRACT

We consider the capabilities of current and future large facilities operating at 2 mm to 3 mm wavelength to detect and image the [CII] 158 μm line from galaxies into the cosmic ‘dark ages’ ($z \sim 10$ to 20). The [CII] line may prove to be a powerful tool in determining spectroscopic redshifts, and galaxy dynamics, for the first galaxies. We emphasize that the nature, and even existence, of such extreme redshift galaxies, remains at the frontier of open questions in galaxy formation. In 40 hr, ALMA has the sensitivity to detect the integrated [CII] line emission from a moderate metallicity, active star-forming galaxy [$Z_A = 0.2 Z_\odot$; star formation rate (SFR) = $5 M_\odot \text{yr}^{-1}$], at $z = 10$ at a significance of 6σ . The next-generation Very Large Array (ngVLA) will detect the integrated [CII] line emission from a Milky-Way like star formation rate galaxy ($Z_A = 0.2 Z_\odot$, SFR = $1 M_\odot \text{yr}^{-1}$), at $z = 15$ at a significance of 6σ . Imaging simulations show that the ngVLA can determine rotation dynamics for active star-forming galaxies at $z \sim 15$, if they exist. Based on our very limited knowledge of the extreme redshift Universe, we calculate the count rate in blind, volumetric surveys for [CII] emission at $z \sim 10$ to 20. The detection rates in blind surveys will be slow (of order unity per 40 hr pointing). However, the observations are well suited to commensal searches. We compare [CII] with the [OIII] 88 μm line, and other ancillary information in high z galaxies that would aid these studies.

Subject headings: galaxies: formation, radio/FIR lines, dust, Lyman Break; cosmic reionization

1. INTRODUCTION

The most sensitive observations with the largest telescopes at γ -ray through radio wavelengths are now discovering galaxies, AGN, and explosive phenomena in the redshift range $z \sim 6$ to 10, some 940 Myr to 500 Myr after the Big Bang. This epoch corresponds to ‘cosmic reionization’, when light from early galaxies and accreting black holes reionized the neutral intergalactic medium (IGM) that pervaded the post-recombination Universe. Measurements of the cosmic microwave background (Planck Collaboration et al. 2016), the Gunn-Peterson effect and related phenomena in the spectra of $z > 6$ quasars (Bañados et al. 2016), the Ly α emission line properties of $z > 6$ galaxies (Ouchi et al. 2017), and most recently, limits to the HI 21cm emission from the neutral IGM at $z > 6$ (Parsons et al. 2014; Ali et al. 2015), are narrowing the redshift range for cosmic reionization. It is becoming clear that the $z \sim 6$ to 10 range corresponds to the period during which the IGM transitions from mostly neutral, to highly ionized, driven by early galaxy formation (Fan et al. 2006; Robertson et al. 2015; Greig & Mesinger 2017; Dayal et al. 2017).

With the advent of the James Webb Space Telescope (*JWST*) and 30m-class ground-based optical and near-IR telescopes, as well as implementation of the full fre-

quency range and capabilities of the Atacama Large Millimeter Array (ALMA), we expect this important period of Universal evolution to be well characterized over the coming decade.

What lies beyond? As we move toward the middle of the 21st century, the redshift frontier will push back to $z \sim 10$ to 20, corresponding to the epoch when the first stars and black holes form, beginning the process of reionization, thereby ending the cosmic Dark Ages (Loeb & Furlanetto 2013).

In this paper we explore the possibility of studying $z = 10$ to 20 galaxies using the 158 μm fine structure line of ionized Carbon with existing and future facilities operating at mm wavelengths. Specifically, we consider the capabilities of the ever-improving ALMA, as new receiver bands open the relevant redshift windows on the [CII] line, in particular in the $z \sim 10$ –15 range. Pushing even further out, to $z \sim 15$ –20, we consider the capabilities of the ‘Next Generation Very Large Array’ (ngVLA) – a facility being considered for 2030 and beyond. The ngVLA takes the next order-of-magnitude leap in sensitivity and resolution relative to the current cm and mm facilities, required to study these first galaxies (Selina & Murphy 2017; Carilli et al. 2015; McKinnon et al. 2016).

The $z \sim 15$ Universe is at the edge of our current understanding. A handful of theoretical studies have speculated on the cosmic star formation rate (SFR) density at these redshifts, in the context of early reionization (Mashian et al. 2016; Duffy et al. 2017; Chary & Pope 2010; Dayal et al. 2014; Yue et al. 2015; Topping & Shull 2015). The main difference with lower redshift galaxy formation scenarios is probably related to lower dynamical masses characterizing earlier structures. This fact makes them much more susceptible to supernova feedback which could partially or totally suppress their star formation via gas ejection and heating. In addi-

¹ National Radio Astronomy Observatory, P. O. Box 0, Socorro, NM 87 801, USA; ccarilli@nrao.edu

² Astrophysics Group, Cavendish Laboratory, JJ Thomson Avenue, Cambridge CB3 0HE, UK

³ National Radio Astronomy Observatory, 520 Edgemont Road, Charlottesville, VA 22901, USA

⁴ Scuola Normale Superiore, Piazza dei Cavalieri 7, I-56126 Pisa, Italy

⁵ Kavli IPMU, The University of Tokyo, 5-1-5 Kashiwanoha, Kashiwa 277-8583, Japan

⁶ Kapteyn Astronomical Institute, University of Groningen, P.O. Box 800, 9700 AV Groningen, The Netherlands

tion, radiative feedback due to photo-ionizing radiation emitted by nearby sources increases the Jeans length in the intergalactic medium, therefore hampering the formation of the smallest galaxies with circular velocities below $\approx 50 \text{ km s}^{-1}$ (Yue et al. 2016; Castellano et al. 2016). All these effects become increasingly important towards higher redshift.

Existing constraints on extreme redshift galaxies are poor, based on extrapolation of the few galaxies and AGN known at $z \sim 7$ to 8, and the even fewer galaxy candidates at $z \sim 8$ to 11. An encouraging observation is the indication of a relatively mature interstellar medium and active star formation, in a few of the extreme redshift sources discovered to date. A very recent result is the detection of the dust continuum and [OIII] $88\mu\text{m}$ fine structure line emission from a candidate galaxy at $z = 8.4$ (Laporte et al. 2017). The galaxy is lensed modestly ($\mu \approx 2$), with an intrinsic star formation rate of $20 M_{\odot} \text{ yr}^{-1}$, a stellar mass of $2 \times 10^9 M_{\odot}$, and a dust mass of $6 \times 10^6 M_{\odot}$. The star formation rate to stellar mass ratio places this galaxy more than an order of magnitude above the standard ‘main sequence’ for star-forming disk galaxies in the nearby Universe. The most extreme redshift candidate remains the $z \sim 11$ galaxy of Oesch et al. (2016). If the source is at the stated redshift, the stellar mass is $\sim 10^9 M_{\odot}$, and the star formation rate is $24 M_{\odot} \text{ yr}^{-1}$. While encouraging, observations remain sparse and uncertain, and the most basic questions remain on the nature, and even existence, of galaxies at $z \sim 15$.

Given the uncertainty in our knowledge of galaxies at extreme redshifts, in this paper we focus on a few simple questions: if such extreme redshift galaxies exist, what kind of facility is required to detect, and possibly image, the [CII] $158\mu\text{m}$ line emission? How do the prospects depend on basic galaxy properties, such as metallicity and star formation rate? Based on what little we know of galaxy demographics at very early epochs, what kind of numbers can we expect in blind cosmological spectral deep fields? We do not consider lensing as a tool, but make the obvious point that lensing can only help go to fainter galaxies (e.g., Gullberg et al. 2015)

The paper is organized as follows: In §2 we describe the importance of the [CII] $158\mu\text{m}$ fine structure and its promise as a way to identify and characterize galaxies at $z \gtrsim 10$. Then, in §3 we describe existing and future telescope capabilities to detect such high- z galaxies. Our results and the implications are presented and discussed in §4. Finally, our main conclusions are then summarized in §5. All calculations are made assuming a Hubble constant $H_0 = 71 \text{ km s}^{-1} \text{ Mpc}^{-1}$ and a flat Λ CDM cosmology with $\Omega_M = 0.27$ and $\Omega_{\Lambda} = 0.73$.

2. WHY THE [CII] $158\mu\text{M}$ LINE?

As we continue to push observations to more and more distant galaxies, the standard rest-frame optical and UV spectral lines used historically to determine redshifts move through the optical into the near-IR windows. At $z > 10$, the $\text{Ly}\alpha$ line redshifts to an observing wavelength $\lambda \geq 1.3\mu\text{m}$, and becomes increasing difficult, or impossible, to observe from the ground. Moreover, even from space, the $\text{Ly}\alpha$ line may be problematic due to the strong resonant damping wings of $\text{Ly}\alpha$ absorption by the pervasive neutral IGM at the end of the Dark Ages (Fan et

al. 2006). Groups have turned their attention to other atomic rest-frame UV-lines, such as CIII] 1907, 1909 and [OII] 3726, 3729 (Barrow et al. 2017), to study the first galaxies, in particular in the context of the up-coming *JWST*.

In this paper, we consider millimeter observations, and using the [CII] $158\mu\text{m}$ line. The [CII] $158\mu\text{m}$ line is typically the brightest of all spectral lines from star-forming galaxies at far-infrared wavelengths and longer (although see §4.5), carrying between 0.1% to 1% of the total far infrared luminosity of star forming galaxies (Stacey et al. 1991). The [CII] fine structure line traces both neutral and ionized gas in galaxies, and is the dominant coolant of star-forming gas in galaxies (Pineda et al. 2013; Velusamy et al. 2015; Langer et al. 2014). Moreover, while the line is only visible from space in the nearby Universe, it becomes easier to observe with increasing redshift, moving into the most sensitive bands of large ground based millimeter telescopes, such as NOEMA⁷, and the ALMA⁸.

The last few years have seen an explosion in the number of [CII] detections at high redshift, including high resolution imaging of the gas dynamics on kpc-scales in distant galaxies. The [CII] line is now routinely detected in both AGN host galaxies and in more normal star-forming galaxies at $z \sim 5.5$ to 7.5 (Willott et al. 2015; Jones et al. 2017; Pentericci et al. 2016; Capak et al. 2015; Maiolino et al. 2015; Venemans et al. 2016; Carilli & Walter 2013; Bradač et al. 2017; Riechers et al. 2013, 2017; Watson et al. 2015; Gullberg et al. 2015; Strandet et al. 2017; Decarli et al. 2016).

Another important characteristic of the [CII] $158\mu\text{m}$ line is that the ratio of [CII] luminosity to far-IR dust continuum luminosity increases with decreasing metallicity (Pineda et al. 2013). The simple point is that, once even a small amount of Carbon is present, it becomes the dominant gas cooling line, hence balancing the heating by star formation.

Considering emission line strength relative to the dust continuum emission and the broad band sensitivity, the [CII] line-to-continuum ratio (in terms of flux density), for $z \sim 6$ galaxies, has been observed to be between 10 and 50 (Willott et al. 2015; Capak et al. 2015; Pentericci et al. 2016). The bandwidth for the line will be limited to the line width, of order 100 km s^{-1} , or some 40 MHz at 110 GHz observing frequency. Modern spectrometers are achieving tens of GHz bandwidth, so the sensitivity is roughly $1000^{1/2}$ better in the dust continuum, or a factor 30. Hence, the detection capabilities might be comparable for the line and continuum. However, we focus on the [CII] line and not dust continuum for the following reasons. First, the formation of dust within 500 Myr of the Big Bang remains highly uncertain, certainly not via mass loss from evolved AGB stars (Michałowski et al. 2010; Dwek 2014; Marassi et al. 2015; Schneider et al. 2015). Carbon is an α element, and hence rapid ISM enrichment from the first generation of massive stars is plausible on timescales $\leq 100 \text{ Myr}$. And second, the goal is not just to detect the galaxy, but to determine its redshift, and possibly the dynamics of the first galaxies.

⁷ <http://iram-institute.org/EN/noema-project.php>

⁸ <http://www.almaobservatory.org>

2.1. [CII] Luminosity, Metallicity, Star Formation, Redshift Relations

As a predictor for the [CII] 158 μm luminosity from early galaxies we use the Vallini et al. (2015) relationship (their Equation 12). This theoretical and observational analysis considers in detail the relationships between star formation rate, galaxy metallicity, and [CII] luminosity to date. We adopt a few representative galaxy characteristics, including the main parameters of: star formation rate, metallicity, redshift, and [CII] luminosity, and compare these to the capabilities of the given facilities. We emphasize that the detailed relationship between [CII] 158 μm luminosity and star formation rate is complex, and remains an area of active debate in the literature, in particular at high redshift (Dias-Santos et al. 2017; De Looze et al. 2014; Olsen et al. 2017).

One of the chief unknowns is the metallicity of very early galaxies. The obvious assumption would be low metallicity. However, there is growing evidence for rapid build-up of metals in the early Universe, at least in the denser regions of active structure formation. Quasars are seen with super-solar metallicity to $z \geq 6$ (Juarez et al. 2009). Likewise, there are galaxies, and galaxy candidates, with well developed ISM characteristics, as seen through dust, CO, and atomic fine structure line emission, at $z \sim 7$ to 8.4 (Venemans et al. 2016; Laporte et al. 2017; Riechers et al. 2017; Watson et al. 2015).

In terms of current calculations of early galaxy formation, the metallicity of the ISM of early galaxies is the ratio between the mass of heavy elements produced by the stellar population and the hydrogen mass, therefore being directly linked to the total mass of stars formed over their assembly. As an example, we consider a galaxy of a halo mass $M_h = 10^8 M_\odot$, corresponding to a 2σ fluctuation at $z = 10$. Assuming a cosmological baryonic-to-dark matter ratio equal to Ω_B/Ω_M , a conversion efficiency of the gas into stars of $e^* = 0.03$ appropriate for early galaxies (Dayal et al. 2017), and further taking the average metal yield per stellar mass formed to be $y = 0.1 M_\odot$, we then get a gas metallicity which depends only on the two last quantities, $Z = ye^* = 3 \times 10^{-3}$, or $Z \approx 0.15 Z_\odot$, essentially independent of halo mass or redshift. This simple estimate assumes that metals and gas are perfectly mixed in the galaxy and do not escape from it via outflows (i.e. a closed-box solution), so it is perhaps an upper limit to Z for a given efficiency/yield. Such a situation is similar to what observed in the BLR of high redshift quasars which always show a relatively high, close to solar, metallicity even at very early times. This argument is further supported by zoom-in numerical simulations (Pallottini et al. 2017), or large scale ones (Wilkins et al. 2017). The latter paper shows that for the smallest halos they can resolve (stellar mass = $10^8 M_\odot$), going from $z = 13$ to $z = 8$, the gas metallicity is bound in the range $-3.03 \leq \log Z \leq -2.95$. Finally, as Carbon is rapidly produced in less than 100 Myr by both pair-instability SNe and AGB stars, the time constraint is relatively easy to achieve: a halo observed at $z = 15$ must have formed the first stars only by $z = 20$.

Overall, the most likely scenario is that the very early Universe is highly inhomogeneous on sub-Mpc-scales, with the densest regions building up metals quickly, and lower density regions remaining pristine (Wilkins et al.

TABLE 1
FACILITIES

Facilities	Redshifts	Frequencies (GHz)	rms ^a ($\mu\text{Jy beam}^{-1}$)	Bandwidth (GHz)
ngVLA	15 – 20	116 – 90	2.0	40
ALMA	10 – 15	173 – 116	21	8 (32 ^b)

^a rms per channel in 40 hr on-source and 100 km s⁻¹ channel.

^b 32GHz is a possible future upgrade to ALMA

2017). In the present analysis we investigate a similarly wide metallicity range to that used in Vallini et al. (2015), i.e., $Z_A \sim 0.04, 0.2$, and $1.0 Z_\odot$.

3. TELESCOPES

In the following section we consider the relevant capabilities for the Atacama Large Millimeter Array, and the planned next generation Very Large Array to detect the [CII] 158 μm line at $z \gtrsim 10$ (see Table 1).

3.1. ALMA

We assume that all the ALMA bands will be completed. In this case, the relevant bands are 3, 4, and 5, corresponding to frequencies of 84 – 116 GHz, 125 – 163 GHz, and 163 – 211 GHz, respectively. These bands then cover the [CII] line (1900.54 GHz rest frequency), between $z = 10$ and 20, almost continuously. There is a gap due to atmospheric O₂ absorption at 118 GHz with a width of a few MHz, and a second strong atmospheric water line at 183 GHz, with about twice the width. The maximum frequency we consider is 173 MHz. The current bandwidth for ALMA is 8 GHz, although an increase to 32GHz is being considered as a future development.

For ALMA sensitivity, we employ the ALMA sensitivity calculator, under good weather conditions (3rd octile), with 50 antennas. For the sake of illustration, we adopt a fiducial line width of 100 km s⁻¹ (see below), an on-source integration time of 40 hr⁹, and a nominal observing frequency of 110 GHz. In this case, the system temperature is $T_{\text{sys}} \approx 75$ K, and the rms sensitivity per channel is 21 $\mu\text{Jy beam}^{-1} \text{ channel}^{-1}$. Adopting the best weather (1st octile), only decreases T_{sys} to ≈ 73 K. The sensitivity of the array degrades with increasing frequency, due to changing system temperature and system efficiency. However, the line width also increases with frequency, in terms of MHz for a fixed velocity width. These factors roughly offset over the frequency range in question, implying comparable sensitivity across the frequency range to within 10%. For simplicity, we adopt the value at 110 GHz. Lastly, we note that ALMA has multiple configurations, all of which are designed to achieve a roughly Gaussian synthesized beam shape for natural weighting of the visibilities (= optimal sensitivity). We assume that the ALMA array chosen is optimized for signal detection of the integrated emission from the galaxies.

3.2. A Next-Generation VLA

⁹ Heretofore, all observing times quoted are on-source observing time. Typical calibration overheads run at around 30% to 40%

The ngVLA is being considered as a future large radio facility operating in the $\sim 1.2 - 116$ GHz range¹⁰. The current design involves ten times the effective collecting area of the JVLA and ALMA, with ten times longer baselines (~ 300 km) providing milliarcsecond resolution, plus a dense core on a 1 km-scale for high surface brightness imaging. The ngVLA opens unique new parameter space for imaging thermal emission from cosmic objects ranging from protoplanetary disks to distant galaxies, as well as unprecedented broad band continuum polarimetric imaging of non-thermal processes (McKinnon et al. 2016; Carilli et al. 2015).

We employ the “Southwest” configuration – one of the proposed configurations for the ngVLA (Carilli et al. 2015, Greisen, Owen, & Carilli *in prep*). This array has 300 antennas distributed across New Mexico, Chihuahua, and Texas. The array includes 40% of the antennas in a core of diameter ~ 1 km, centered on the VLA site. Then some 30% of the antennas out to VLA A-array baselines of 30 km, and the rest to baselines as long as 500 km, into Northern Mexico and Texas to enable AU-scale imaging of protoplanetary disks in nearby star-forming regions.

For the ngVLA noise calculation, we adopt the interferometric radiometer equation (Thompson et al. 2017), using an 18 m diameter antenna, with 70% efficiency, 80 K system temperature, a 40 hr observation, and a 100 km s^{-1} channel width. We assume observations from 90 – 115 GHz, implying a redshift range for [CII] of $z \sim 15$ to 20. The ngVLA bandwidth will cover this entire range instantaneously. Under these assumptions, we calculate a naturally-weighted noise level of $1.3 \mu\text{Jy beam}^{-1} \text{ channel}^{-1}$.

While the issue of reconfiguration of the ngVLA remains open, for this exercise we conservatively assume a non-reconfigurable array. The current design of the ngVLA has a very non-uniform antenna distribution. The naturally-weighted beam for this centrally condensed distribution leads to a PSF with a high resolution core of a few mas width at 90 GHz, plus a broad, prominent pedestal or plateau in the synthesized beam with a response of $\sim 50\%$ over $\sim 1''$ scale. The goal in imaging is to adjust the relative weighting of the data on different baselines lengths to obtain the best the sensitivity, while maintaining a well behaved synthesized beam (point spread function), relative to expected source sizes (likely a few kpc, or $0'.1$ to $1''$). In our array simulations below, we find that such a compromise can be reached on angular scales relevant to the expected source sizes ($\sim 0'.2$ to $0'.4$), with a loss of about a factor ~ 1.5 in sensitivity relative to natural (optimal) weighting (Carilli et al. 2015).

3.3. Simulations and Galaxy Parameters

For the purpose of estimating the sensitivity of the ngVLA for realistic observations, and to explore the imaging capabilities in the event of the discovery of any relatively luminous sources, we have employed the CASA simulation tools (Carilli et al. 2015, 2017), developed for the ngVLA project¹¹. We simulate a 40 hr observation, made up of a series of 4 hr scheduling blocks around tran-

sit.

For imaging, we employ the CLEAN algorithm with Briggs weighting. We adjust the ROBUST parameter, the (u, v) -taper, and the cell size, to give a reasonable synthesized beam and noise performance. Our target resolution is $\sim 0'.4$ for detection, and $\sim 0'.2$ for imaging. The latter corresponds to 0.6 kpc physical, at $z = 15$.

We adopt as a spatial and dynamical template, the observed CO 1-0 emission from the nearby star-forming disk galaxy, M51. M51 is one of the best studied galaxies in cool gas dynamics (Helfer et al. 2003; Schinnerer et al. 2013) with a total observed line width of about 150 km s^{-1} , and a disk radius in CO of about 5 kpc. We assume that rotational dynamics is the same for all gas constituents (e.g., CO or [CII]). We also arbitrarily reduce the physical size of the disk by a factor three, with the idea that very early galaxies are likely smaller than nearby galaxies. Again, this exercise is for illustrative purposes, and the input model is just a representative spatial/dynamical template for a disk galaxy, with the relevant parameters being size, velocity, and luminosity. We employ the publicly available BIMA SONG CO 1-0 data cubes (Helfer et al. 2003), as the starting point of the models. These data have high spatial resolution (37 pc) and excellent signal to noise.

We then adjust the line luminosity per channel per beam, to achieve a given integrated [CII] $158 \mu\text{m}$ luminosity at a given redshift. The predicted luminosities as a function of basic galaxy properties are discussed in the following section.

4. RESULTS

In this section we present the results of our analysis to both detect and characterize $z \gtrsim 10$ galaxy candidates using ALMA and the ngVLA, as well as searching for such high- z sources via their [CII] emission.

4.1. Spectroscopic Confirmation of $z \gtrsim 10$ Candidates

An obvious application of the [CII] $158 \mu\text{m}$ line search will be to determine spectroscopic redshifts for near-IR dropout candidate galaxies at $z \sim 10$ to 20. Such spectroscopic verification using [CII] may prove to be a powerful method to study of the earliest galaxies, allowing for wideband searches and possible high resolution imaging of the gas dynamics. The metallicity of these galaxies remains an open issue, but on the positive side, the galaxies most likely to be first discovered as near-IR dropouts by *JWST*, either in targeted deep fields or serendipitously, will be the most prodigiously star-forming galaxies. These will then be the easiest to detect with the ngVLA and ALMA in their [CII] emission.

We start with the relationship between the [CII] velocity integrated line flux, in the standard flux units of Jy km s^{-1} , versus redshift. We adopt a metallicity of $Z_A = 0.2 Z_\odot$, and star formation rates of $1 M_\odot \text{ yr}^{-1}$ and $5 M_\odot \text{ yr}^{-1}$. Figure 1 shows the predicted [CII] line flux versus redshift for the two models, along with the 1σ sensitivity of ALMA and the ngVLA. Again, we note that for ALMA we adopt optimal (naturally weighted) sensitivity, assuming an appropriate configuration is used for detection. For the ngVLA, we have degraded the sensitivity by a factor 1.5 from optimal, due to requirements of visibility weighting to obtain a reasonable PSF (see §3.2).

¹⁰ <https://science.nrao.edu/futures/ngvla>

¹¹ <https://science.nrao.edu/futures/ngvla/documents-publications>

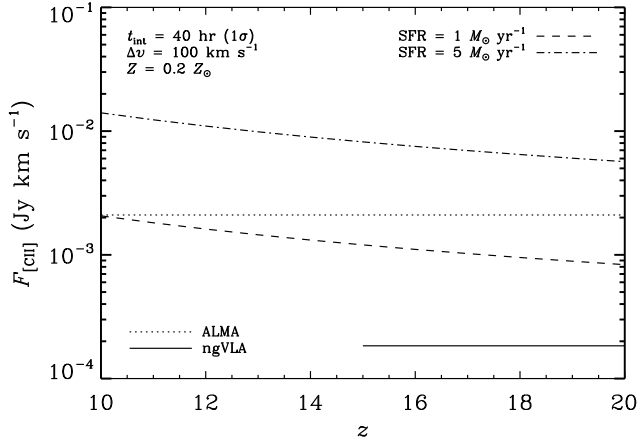


FIG. 1.— [CII] $158 \mu\text{m}$ velocity integrated line flux versus redshift for galaxies with star formation rates of $1 M_{\odot} \text{yr}^{-1}$ and $5 M_{\odot} \text{yr}^{-1}$, and metallicity of $0.2 Z_{\odot}$, based on the relationship given in Equation 12 of Vallini et al. (2015). The rms sensitivity in a 100 km s^{-1} channel and 40 hr integration is shown for both ALMA and the ngVLA.

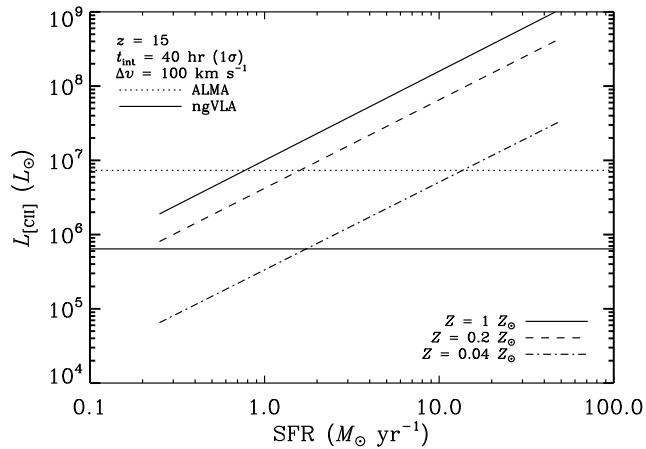


FIG. 2.— [CII] $158 \mu\text{m}$ line luminosity versus star formation rate and metallicity, based on the relationship given in Equation 12 of Vallini et al. (2015). Three different metallicities are shown. Also shown is the rms sensitivity of ALMA and the ngVLA for a galaxy at $z = 15$, assuming a 100 km s^{-1} channel and 40 hr integration.

In 40 hr, the ngVLA will be able to detect the integrated [CII] line emission from moderate metallicity and star formation rate galaxies ($Z_A = 0.2$, $\text{SFR} = 1 M_{\odot} \text{yr}^{-1}$), at $z = 15$ at a significance of 6σ . This significance reduces to 4σ at $z = 20$.

In 40 hr, ALMA will be able to detect the integrated [CII] line emission from a higher star formation rate galaxy ($Z_A = 0.2 Z_{\odot}$, $\text{SFR} = 5 M_{\odot} \text{yr}^{-1}$), at $z = 10$ at a significance of 6σ . This significance reduces to 4σ at $z = 15$. ALMA will be hard-pressed to detect a moderate metallicity ($Z_A = 0.2 Z_{\odot}$), lower star formation rate ($1 M_{\odot} \text{yr}^{-1}$) galaxy, requiring 1000 hr for a 5σ detection of the velocity integrated line flux, even at $z = 10$.

We next consider dependence on metallicity. Figure 2 shows the relationship between [CII] luminosity (in Solar units), to star formation rate, for three different metallic-

ities: $Z_A = 0.04, 0.2$, and $1.0 Z_{\odot}$, for a galaxy at $z = 15$. Again shown are the ALMA and ngVLA sensitivities in 40 hr, 100 km s^{-1} channels. The Vallini et al. (2015) model has the [CII] luminosity as a strong function of metallicity. If the gas has Solar metallicity, the ALMA detection threshold (4σ) reduces to a galaxy with a star formation rate of $2.5 M_{\odot} \text{yr}^{-1}$ (compared to $5 M_{\odot} \text{yr}^{-1}$ for $Z_A = 0.2$), while that for the ngVLA reduces to $0.4 M_{\odot} \text{yr}^{-1}$ (compared to $1 M_{\odot} \text{yr}^{-1}$ for $Z_A = 0.2$). Conversely, for a low metallicity galaxy of $Z_A = 0.04 Z_{\odot}$, these values increase to $100 M_{\odot} \text{yr}^{-1}$ and $10 M_{\odot} \text{yr}^{-1}$, respectively.

Consequently, it appears that ALMA should be able to spectroscopically confirm drop-out candidate galaxies forming stars at a rate of a few solar masses per year with metallicity ≥ 0.2 at $z \sim 10$, in reasonable integration times. The ngVLA pushes this detection limit to $z \sim 15$ to 20, for star formation rates of order unity with $Z_A \geq 0.2$. If such galaxies do exist, ALMA and the ngVLA should be excellent tools to confirm their existence.

4.2. Kinematics of $z \gtrsim 10$ Galaxies

We investigate the potential for obtaining kinematic information from such galaxies using the ngVLA. We start by considering visibility weighting to obtain a detection of the integrated emission from a high redshift galaxy with the configuration of the ngVLA. The imaging is a complex optimization procedure, balancing the Briggs ROBUST weighting parameter (Briggs 1995), the Gaussian tapering of the (u, v) -weighting, and the cell size in the gridding kernel, to approach a reasonable balance between good sensitivity and the behaviour of the PSF. Pure natural weighting for the ngVLA leads to a PSF ‘core’ of just a few milliarcseconds due to the 300 km baselines, which radically over-resolves the emission. See Carilli (2016) for more details on imaging optimization using the suite of current tools in CASA.

We have explored a few of the main parameters using the tools available, with a goal of getting a rough estimate of the loss of sensitivity when imaging with non-optimal array configurations. We expect the search for optimal imaging techniques for various goals (simple detection or high resolution imaging), to be a long-term exercise in interferometric imaging, with the advent of the complex array configurations envisioned for facilities such as the ngVLA and the Square Kilometer Array. Our current estimates of sensitivity are likely conservative, depending on future algorithmic development.

For reference, Figure 3 shows results for the input galaxy model we use to explore the imaging parameters, as discussed in §3.3. In this case, we have imaged the source with no noise added, and using imaging parameters that result in a PSF with a FWHM = $0''.1$, in order to show the intrinsic properties of the model galaxy. We show both the velocity integrated [CII] emission, and the intensity weighted mean [CII] velocity. The model shows spiral arms extending over an area of about $\sim 0''.4$, with the majority of the emission centrally condensed bar and nucleus in the inner $\sim 0''.2$.

Figure 4 shows the image of the velocity integrated [CII] line emission from the $Z_A = 0.2 Z_{\odot}$, and $\text{SFR} = 1 M_{\odot} \text{yr}^{-1}$ galaxy, assuming noise appropriate for a 40 hr observation. We adopt imaging parameters that opti-

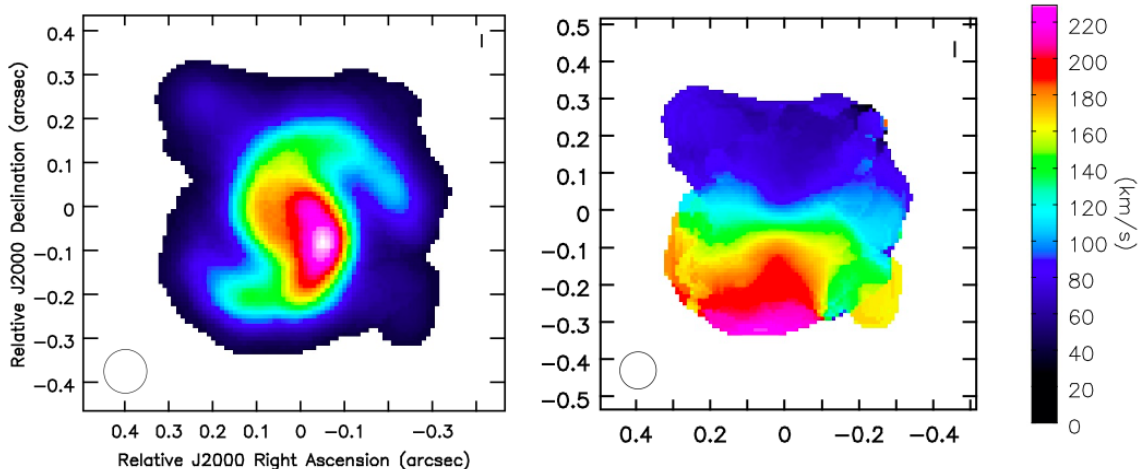


FIG. 3.— *Left*: A simulated image of the velocity integrated [CII] $158\ \mu\text{m}$ emission from a $z = 15$ galaxy with a star formation rate of $5 M_{\odot}\ \text{yr}^{-1}$, and a metallicity of $0.2 Z_{\odot}$. In this case, no noise is added to the simulation, but the weighting applied to the visibilities was set to achieve a synthesized beam of $\text{FWHM} = 0''.1$, to obtain a better view of the intrinsic gas distribution of the model. *Left* is the velocity integrated line emission. *Right*: The intensity weighted mean [CII] velocity (moment 1).

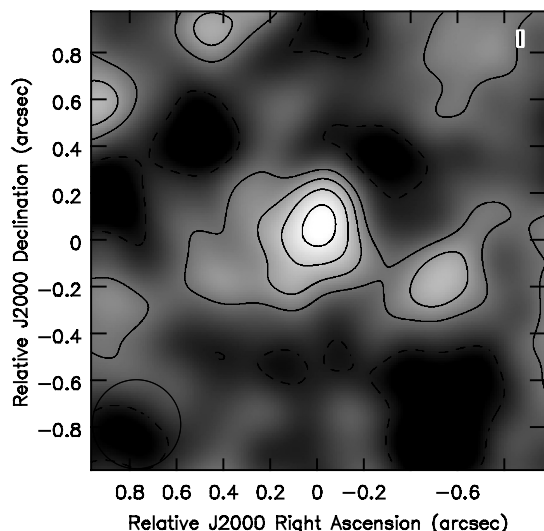


FIG. 4.— A simulated image of the velocity integrated [CII] $158\ \mu\text{m}$ emission from a $z = 15$ galaxy with a star formation rate of $1 M_{\odot}\ \text{yr}^{-1}$, and a metallicity of $0.2 Z_{\odot}$, assuming for a 40 hr observation with the ngVLA. The contour levels are -3.2, -1.6, 1.6, 3.2, 4.8, $6.4\ \mu\text{Jy beam}^{-1}$. The rms noise on the image is $1.6\ \mu\text{Jy beam}^{-1}$, and the synthesized beam FWHM is $0''.38$.

mize detection of the integrated emission. The emission is clearly detected using Briggs weighting with $\text{ROBUST} = 1$, a Gaussian (u, v) -taper of $0''.2$, and a cell size of $0''.01$. This yields a beam $\text{FWHM} \sim 0''.4$ and an rms of $1.6\ \mu\text{Jy beam}^{-1}$ over the $150\ \text{km s}^{-1}$ velocity range (or about $2\ \mu\text{Jy beam}^{-1}$ at $100\ \text{km s}^{-1}\ \text{channel}^{-1}$, compared to $1.3\ \mu\text{Jy beam}^{-1}$ for natural weighting of the visibilities). The result is about a 5.5σ detection of the integrated emission from Gaussian fitting.

We next consider imaging of the higher star formation rate model, with $Z_A = 0.2 Z_{\odot}$, and $5 M_{\odot}\ \text{yr}^{-1}$ galaxy for a 40 hr observation. Given the brighter signal, we investigate whether information on the gas dynamics can be recovered with high resolution imaging. We employ Briggs weighting with $\text{ROBUST} = 0.5$, a Gaussian (u, v) -taper of $0''.15$, and a cell size of $0''.01$. This yields a beam $\text{FWHM} \sim 0''.2$. We synthesize channel images at $20\ \text{km}$

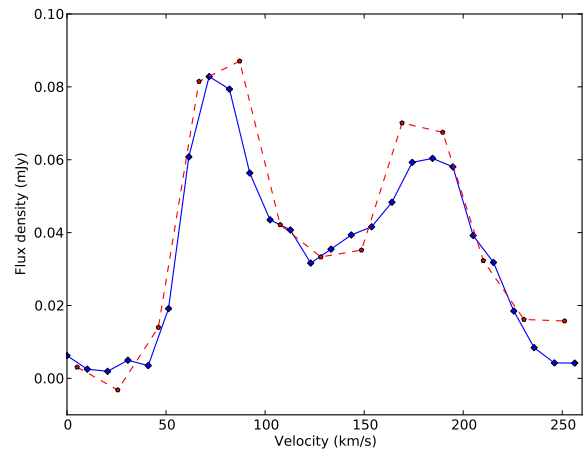


FIG. 5.— The red dashed line shows a simulated spectrum of the spatially integrated [CII] $158\ \mu\text{m}$ emission from a $z = 15$ galaxy with a star formation rate of $5 M_{\odot}\ \text{yr}^{-1}$, and a metallicity of $0.2 Z_{\odot}$, assuming for a 40 hr observation with the ngVLA, at $20\ \text{km s}^{-1}\ \text{channel}^{-1}$. The blue line shows the same spectrum, but with no noise added and at $10\ \text{km s}^{-1}\ \text{channel}^{-1}$.

$\text{s}^{-1}\ \text{channel}^{-1}$, for which the rms noise is about $4.5\ \mu\text{Jy beam}^{-1}$. We also generate a velocity integrated [CII] image averaging over the full width of the line.

The resulting spectrum, integrated over the source area, is shown in Figure 5. The red dash line is the simulated spectrum at $20\ \text{km s}^{-1}\ \text{channel}^{-1}$ with noise added, while the blue line shows the integrated line emission made from data with no noise added, and at $10\ \text{km s}^{-1}\ \text{channel}^{-1}$, as a reference spectrum (Fig 3). Clearly, the ngVLA can make a high signal to noise detection of the emission from this galaxy, with an integrated significance for the detection of about 20σ .

From the channel images we generate the intensity weighted mean velocity image (moment 1), using surface brightnesses above 2σ . The result is shown Figure 6. The velocity integrated intensity, and mean velocity, images can be compared to Figure 4, which again shows the same model, but with noiseless (u, v) data, and at

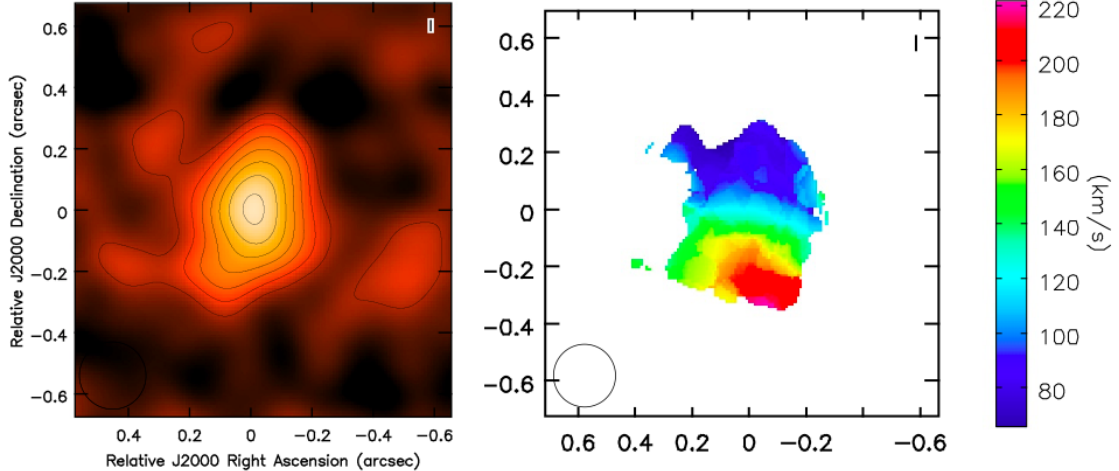


FIG. 6.— *Left:* A simulated image of the velocity integrated [CII] $158\ \mu\text{m}$ emission from a $z = 15$ galaxy with a star formation rate of $5\ M_{\odot}\ \text{yr}^{-1}$, and a metallicity of $0.2\ Z_{\odot}$, assuming for a 40 hr observation with the ngVLA. Left is the velocity integrated line emission. The contour levels are -6, -3, 3, 6, 9, 12, 15, 18, $21\ \mu\text{Jy beam}^{-1}$. The rms noise on the image is about $1.8\ \mu\text{Jy beam}^{-1}$, and the synthesized beam FWHM is $0''.22$. *Right:* The intensity weighted mean [CII] velocity (moment 1).

higher spatial resolution. Clearly, at this signal to noise and resolution we cannot recover the detailed structure of the gas, such as the spiral arm features. However, the overall velocity gradient is recovered, including the maximum and minimum velocity of the gas, as well as the north-south orientation and extension of the major axis.

4.3. The Potential for Blind Searches of $z \gtrsim 10$ Galaxies

Another application for the [CII] line will be blind cosmological deep fields. The advent of very wide bandwidth spectrometers has led to a new type of cosmological deep field, namely, spectral volumetric deep fields, in which a three dimensional search for spectral lines can be made, with redshift as the third dimension (e.g., Walter et al. 2016).

To this aim we consider two predictions for the number density of galaxies at these very high redshifts from the recent literature. These predictions employ very different methodologies. Again, we point out that the current observational constraints are extremely limited. Both models employ a Salpeter IMF from 0.1 to $100\ M_{\odot}$.

First, we consider the galaxy number counts of Chary & Pope (2010, CP10). These galaxy counts are based on backward-evolving models for the infrared luminosity function of Chary & Elbaz (2001), anchored by a variety of observational data including the deepest *Spitzer* $24\ \mu\text{m}$ imaging from the GOODS fields, the fraction of the far-infrared background light resolved by *Spitzer* and *Herschel*, spectroscopic redshifts of *Spitzer* and *Herschel* sources in the deep fields, and are consistent with the number counts as well as $P(D)$ analysis from deep *Herschel* observations.

Second, we employ the calculation of high redshift galaxy formation of Dayal et al. (2014, Dayal14). This model aims at isolating the essential physics driving early galaxy formation via a merger-tree based semi-analytical model including the key physics of star formation, supernova feedback and the resulting gas ejection, and the growth of progressively more massive systems (via halo mergers and gas accretion). It involves only two free pa-

rameters, the star formation efficiency threshold, f_* , and the fraction of SN energy that drives winds, f_w . The key premise is that any galaxy can form stars with a maximal effective efficiency, f_*^{eff} , that provides enough energy to expel all the remaining gas, quenching further star formation. The value of $f_*^{eff} = \min[f_*, f_*^{ej}]$ where f_*^{ej} is the star-formation efficiency required to eject all gas from a galaxy. Thus, low-mass galaxies form stars at a more limited efficiency than massive galaxies.

The model has been validated against available high- z data. For example, it reproduces extremely well both the slope and amplitude of the UV LF from $z = 5$ to $z = 10$ at the same time providing a physical explanation for the slope evolution in terms of a faster assembly of galaxies at earlier redshifts. Dayal14 also predicts that the bright-end slope of the UV LF should be flatter than the steep drop-off implied by the Schechter function, and actually closer to the slope of the underlying dark matter halo mass function. This, in turn, might be interpreted as a limited impact of quasar feedback at high redshifts.

The two models predict the cumulative co-moving number density of star-forming galaxies above a given star formation rate as a function of redshift. We show the results in Figures 7a and 7b for the CP10 and Dayal14 models, respectively.

The co-moving number densities can be turned into the number of observed galaxies in a given integration time, bandwidth, and field of view, using the sensitivities of the ngVLA and ALMA. In §4.1, we calculated that, in 40 hr for a galaxy with $Z_A = 0.2$, the ngVLA can detect a $\text{SFR} = 1\ M_{\odot}\ \text{yr}^{-1}$ galaxy at 6σ significance between $z = 15$, reducing to 4σ at $z = 20$. ALMA can detect a $\text{SFR} = 5\ M_{\odot}\ \text{yr}^{-1}$ galaxy at 6σ at $z = 10$, reducing to 4σ significance between $z = 15$. We use these two star formation rates for demonstrative purposes.

Figure 8 shows the number of galaxies per arcmin² per unit redshift for $\text{SFR} \geq 1\ M_{\odot}\ \text{yr}^{-1}$ and $5\ M_{\odot}\ \text{yr}^{-1}$, for the CP10 and Dayal14 models, respectively. The models show markedly different behaviour. The Dayal14 model has much steeper redshift evolution. The Dayal14 model also has a much faster drop in density with increasing

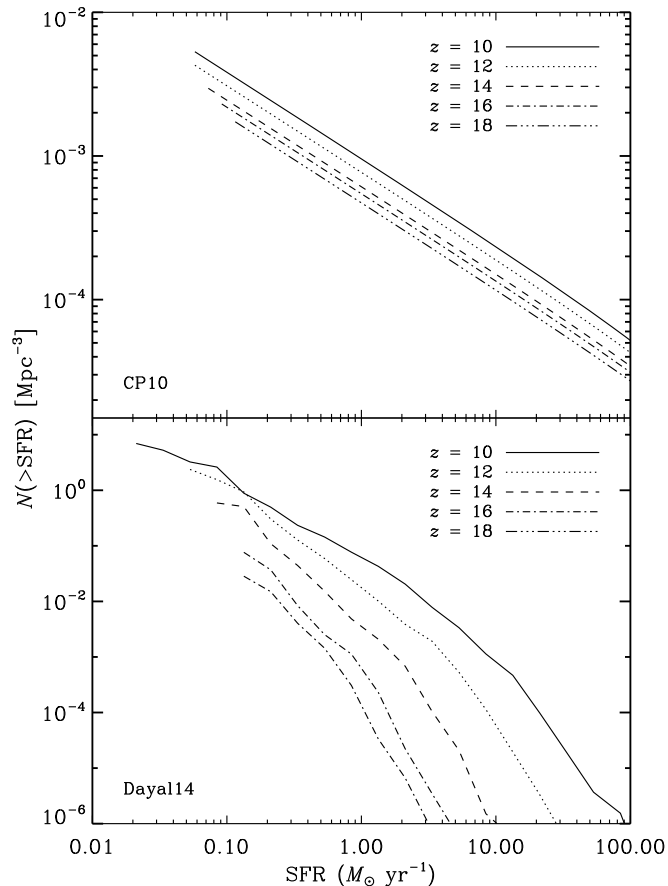


FIG. 7.— Comoving number density of galaxies vs. star formation rate and redshift. The upper plot is the model of Chary & Pope (2010). The lower plot is the Dayal et al. (2014) model.

SFR. Perhaps fortuitously, at $1 M_{\odot} \text{ yr}^{-1}$, the areal densities for the two models cross at $z \sim 15$.

The ngVLA can observe the 90 GHz to 116 GHz bandwidth simultaneously, corresponding to $z = 20$ to 15. We also consider just the number of galaxies between $z = 15$ and 16. ALMA has receivers that will cover from $z = 10$ to 15, or frequencies from 173 GHz to 116 GHz, but different receivers are needed over the full redshift range. Currently, the bandwidth is limited to 8 GHz. We consider an 8 GHz blind search in the Band 5 from 165 GHz to 173 GHz ($z = 10.5$ to 10), and one covering most of Band 4 with a 32 GHz bandwidth, from 126 GHz to 158 GHz ($z = 11$ to 14).

The field of view of the ngVLA at the mean frequency of 100 GHz is $\sim 0.38 \text{ arcmin}^2$, adopting the FWHM of 0.70 arcmin for an 18 m antenna. The field of view of ALMA at the mean frequency of 146 GHz is $\sim 0.39 \text{ arcmin}^2$, adopting the FWHM of 0.71 arcmin for a 12 m antenna.

In Table 2, we tabulate the number of galaxies detected in [CII] emission per 40 hr integration per frequency tuning, for the ngVLA and ALMA, and for the different models. For the ngVLA, and for $\text{SFR} \geq 1 M_{\odot} \text{ yr}^{-1}$, the models predict that one to two independent pointings will be required to detect one galaxy over the full redshift range, on average. For the CP10 model, these

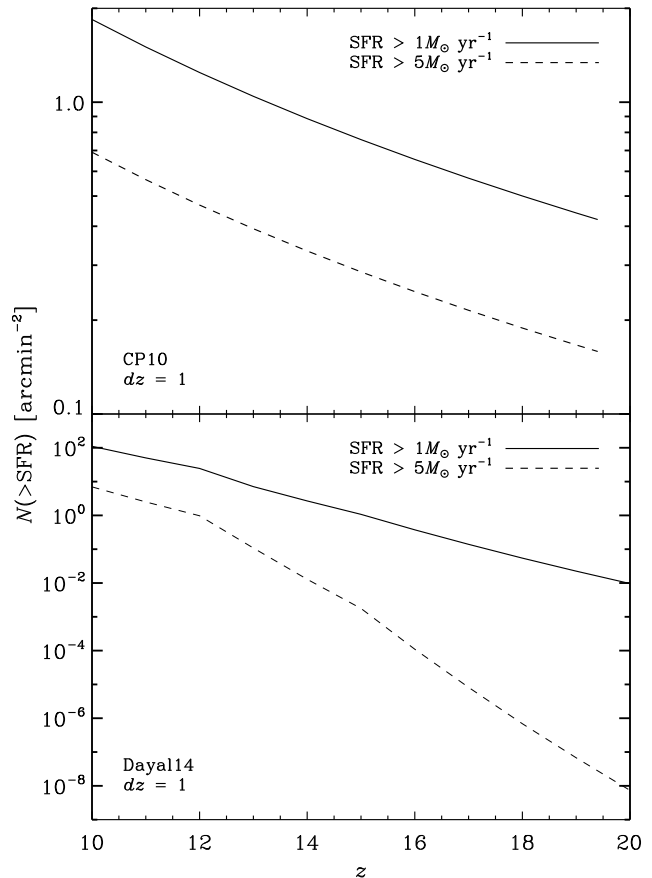


FIG. 8.— Number of galaxies with star formation rates greater than $1 M_{\odot} \text{ yr}^{-1}$ per arcmin^2 per unit redshift, and $5 M_{\odot} \text{ yr}^{-1}$ per arcmin^2 per unit redshift. The upper plot is the model of Chary & Pope (2010). The lower plot is the Dayal et al. (2014) model.

sources have a broader redshift distribution, with 22% of the sources at $z = 15$ to 16. For the Dayal14 model, the majority (64%), of the sources are in this lowest redshift bin.

For ALMA and $\text{SFR} \geq 5 M_{\odot} \text{ yr}^{-1}$, the predicted number of detections differs significantly between models. For the 8 GHz bandwidth search in Band 5 ($z = 10$ to 10.5), the CP10 model requires about three pointings for a single detection, on average, while the Dayal14 model has more low redshift, brighter galaxies, with three sources per pointing expected. For the 32 GHz bandwidth search in Band 4 ($z = 11$ to 14), the values are roughly two pointings needed for a single detection for the CP10 model, and one pointing needed for the Dayal14 model.

Overall, the detection rates in blind surveys will be slow (of order unity per 40 hr pointing). However, the observations are well suited to commensal searches on all programs employing the very wide bands that may be available in future. Perhaps most importantly, the very different predictions of the detection rates with respect to redshift and star formation rate for the two models, both highlights our lack of knowledge of the extreme redshift Universe, and implies that the [CII] results may have great leverage in constraining models of galaxy for-

TABLE 2
NUMBER OF DETECTIONS PER 40 HR POINTING

Model	ngVLA $z = 15$ to 16	ngVLA $z = 15$ to 20	ALMA ^a $z = 10$ to 10.5	ALMA ^b $z = 11$ to 14
CP10, 1 M_{\odot} yr ⁻¹	0.29	1.3	–	–
CP10, 5 M_{\odot} yr ⁻¹	0.11	0.48	0.29	0.68
Dayal14, 1 M_{\odot} yr ⁻¹	0.36	0.64	–	–
Dayal14, 5 M_{\odot} yr ⁻¹	6.9×10^{-4}	7.3×10^{-4}	2.8	1.4

^a Nominal ALMA bandwidth of 8 GHz

^b Proposed ALMA bandwidth upgrade to 32 GHz

mation.

As a final note, we point out that blind surveys would be greatly facilitated by focal plane arrays. This option is being considered for large interferometric arrays, like the ngVLA, ALMA, and NOEMA, although it comes at significant expense.

Large single dish telescopes are also developing large format focal plane arrays operating in these frequency ranges that will be relevant for high redshift [CII] searches. The two single dish telescopes that potentially will have the sensitivity to detect the modest star formation rate galaxies at $z > 10$ considered herein are the Green Bank Telescope (GBT¹²), and the Large Millimeter Telescope (LMT¹³). These telescopes have comparable sensitivity (within a factor two or better), of ALMA at 100 GHz. For example, if a wide-band focal plane array with over 70 elements is deployed at the GBT, the survey speed would then rival, and possibly surpass, ALMA in the 90 GHz to 116 GHz band, depending on bandwidth.

4.4. Verifying sources

A key issue in blind searches is spurious detections and verifying sources. For instance, even just considering thermal noise, the probability for a $\sim 5\sigma$ random positive noise peak is 2.9×10^{-7} . In the ngVLA blind search at 0.4" resolution, the field of view is 37", or a total of 8600 independent synthesized beams per FoV. The total frequency range covered in 26 GHz at a resolution of 100 km s⁻¹, or 33 MHz, hence 780 independent spectral resolution elements. The number of independent voxel elements in the search is then 6.7×10^6 , implying two noise sources by chance. This confusion obviously gets worse at lower significance, and can be exacerbated by non-Gaussian noise errors due to sidelobes from continuum or strong line sources (Aravena et al. 2016).

Recent blind line searches have developed some techniques for making statistical corrections to number counts based on e.g., comparing the number of negative and positive detections at a give level (Decarli et al. 2014; Decarli et al. 2016; Walter et al. 2016; Aravena et al. 2016). However, the problem still remains as to how to verify that a given detection is associated with a $z > 10$ galaxy. For this, other information will be needed.

One possibility will be broad band near-IR colors from e.g., *JWST*, or large ground based telescopes. The capability of the *JWST* to make such measurements has been demonstrated in e.g., (Volonteri et al. 2017). Likewise, follow-up spectroscopy with *JWST* may reveal atomic lines (Barrow et al. 2017). Lastly, ALMA could be used

to search for [OIII] emission, in cases of low metallicity galaxies (see below).

4.5. [OIII] 88 μ m and [CII] 158 μ m

The [OIII] fine structure line at 88 μ m, which traces ionized gas, can be as bright as, or brighter than, the [CII] line in low metallicity galaxies. In their study of nearby galaxies, (Cormier et al. 2015) show the [OIII]/[CII] ratio has a large scatter, but the ratio can occasionally be as large as a factor of ~ 10 . Likewise, ALMA observations of a $z = 7.2$ galaxy show a similar large [OIII]/[CII] ratio, possibly due to a higher ionization state for the gas in the galaxy (Inoue et al. 2016). On average, the median [OIII]/[CII] ratio reported for the entire sample of low-metallicity dwarfs studied by (Cormier et al. 2015) is 2.00 with a dispersion of 0.36 dex. We consider a few examples of the comparative sensitivities herein, adopting this median factor two for low metallicity dwarfs.

For example, consider the redshift search for a target drop-out galaxy at $z \sim 12$ with ALMA. The [OIII] and [CII] lines redshift to frequencies of 260.2 (ALMA Band 6) and 145.8 GHz (ALMA Band 4), respectively. The ALMA sensitivities at these frequencies are similar, with the rms at 260.2 GHz being only $\approx 15\%$ larger than at 145.8 GHz (the increase in system temperature with increasing frequency is offset by the increasing bandwidth for a fixed velocity width line). Hence, a factor two stronger [OIII] line requires a factor ~ 4 less observing time to reach a given signal-to-noise. Countering this factor is the factor 1.8 smaller fraction bandwidth at the higher [OIII] frequency, thereby requiring more frequency tunings in the search.

In terms of blind searches with ALMA itself, again, the factor two brighter [OIII] line vs. [CII] (in the mean for low metallicity dwarf galaxies), then requires a factor four less integration time. However, the primary beam and fractional bandwidth at 145.8 GHz are factors of 3.2 and 1.8 larger than at 260.2 GHz. Hence, the cosmic volume searched at the higher frequency per tuning and pointing is a factor 5.7 larger at the lower frequency, more than off-setting the signal-to-noise gain, although not by a large factor.

Considering ALMA and [OIII] vs. the ngVLA and [CII] at $z = 15.5$, the [OIII] and [CII] lines redshift to frequencies of 205 (ALMA Band 5) and 115 GHz, respectively. The sensitivity at 205 GHz in Band 5 is a factor of ≈ 11 times worse than at 115 GHz with the ngVLA. The primary beam area and fractional bandwidth of the ngVLA at 115 GHz are factors of 1.4 and 5.8 times larger than at 205 GHz with ALMA. The sum total is that ngVLA searches are ≈ 1040 times faster for [OIII]/[CII] = 1. Hence, only if [OIII] is systematically

¹² <http://greenbankobservatory.org/>

¹³ <http://www.lmtgtm.org/>

brighter than [CII] by a factor of ≈ 33 will ALMA in [OIII] be competitive in blind searches relative to the ngVLA in [CII]. It is worth noting that this calculation does not take into account the fact that ALMA Band 5 observations are severely affected by the 183 GHz water line, which essentially wipes out sensitive observations over the frequency range spanning $\sim 175 - 195$ GHz ($18 \leq z \leq 16$ for [OIII]).

Overall, for redshift searches on individual candidate drop-out galaxies, assuming the mean factor two higher signal-to-noise for [OIII] vs. [CII] for low metallicity dwarf galaxies, the [OIII] line may prove more effective a tool in terms of search time, although only marginally since the factor 4 decrease in time due to the stronger signal is offset by the factor 1.8 smaller fractional bandwidth at higher frequency. For blind galaxy searches, the increase in fractional bandwidth, and the increase in field of view, at lower frequency, more than offset the increase in signal to noise, although not by a large margin. It is also important to keep in mind that phase coherence is more of an issue at higher frequency, and hence the [OIII] line will require better weather.

Perhaps most importantly, the various atmospheric windows may preclude searches at different redshifts for the different lines. Having two potential lines to search for is an added bonus.

5. CONCLUSIONS

We have considered observing [CII] $158\mu\text{m}$ emission from $z = 10$ to 20 galaxies. The [CII] line may prove to be a powerful tool to determine spectroscopic redshifts, and galaxy dynamics, for the first galaxies at the end of the dark ages, such as identified as near-IR dropout candidates by *JWST*. We emphasize that the nature, and even existence, of such extreme redshift galaxies, remains at the frontier of studies of galaxy formation.

In 40 hr, the ngVLA has the sensitivity to detect the integrated [CII] line emission from moderate metallic-

ity and (Milky-Way like) star formation rate galaxies ($Z_A = 0.2$, $\text{SFR} = 1 M_\odot \text{yr}^{-1}$), at $z = 15$ at a significance of 6σ . This significance reduces to 4σ at $z = 20$. In 40 hr, ALMA has the sensitivity to detect the integrated [CII] line emission from a higher star formation rate galaxy ($Z_A = 0.2 Z_\odot$, $\text{SFR} = 5 M_\odot \text{yr}^{-1}$), at $z = 10$ at a significance of 6σ . This significance reduces to 4σ at $z = 15$. We also consider dependencies on metallicity and star formation rate. Recent studies suggest that the [CII] luminosity increases rapidly with both metallicity and star formation rate Vallini et al. (see 2013, 2015).

We perform imaging simulations using a plausible model for the gas dynamics of disk galaxies, scaled to the sizes and luminosities expected for these early galaxies. The ngVLA will recover rotation dynamics for active star-forming galaxies ($\gtrsim 5 M_\odot \text{yr}^{-1}$ at $z \sim 15$), in reasonable integration times.

We adopt two models for very high redshift galaxy formation, and calculate the expected detection rate for [CII] emission at $z \sim 10$ to 20, in blind, wide bandwidth, spectroscopic deep fields. The detection rates in blind surveys will be slow (of order unity per 40 hr pointing). However, the observations are well suited to commensal searches on all programs employing the very wide bands that may be available in future. We consider the need for ancillary observations, such as broad band *JWST* colors or ALMA [OIII] $88\mu\text{m}$ line observations, to verify the association of a given line to a $z > 10$ galaxy.

Acknowledgements: PD acknowledges support from the European Research Council's starting grant ERC StG-717001 and from the European Commission's and University of Groningen's CO-FUND Rosalind Franklin program. The National Radio Astronomy Observatory is a facilities of the National Science Foundation operated under cooperative agreement by Associated Universities, Inc.. We thank Ranga-Ram Chary for discussions on the models and the paper.

REFERENCES

- Ali, Z. S., Parsons, A. R., Zheng, H., et al. 2015, *ApJ*, 809, 61
 Aravena, M.; Decarli, R.; Walter, F.; Bouwens, R.; Oesch, P. A. et al. 2016, *ApJ*, 833, 71
 Bañados, E., Venemans, B. P., Decarli, R., et al. 2016, *ApJS*, 227, 11
 Barrow, Kirk S. S.; Wise, John H.; Norman, Michael L.; O'Shea, Brian W.; Xu, Hao 2017, *MNRAS*, 469, 4863
 Briggs, D. 1995, PhD Thesis, New Mexico Institute of Mining and Technology
 Bradač, M., Garcia-Appadoo, D., Huang, K.-H., et al. 2017, *ApJ*, 836, L2
 Capak, P. L., Carilli, C., Jones, G., et al. 2015, *Nature*, 522, 455
 Carilli, C. L., McKinnon, M., Ott, J., et al. 2015, arXiv:1510.06438 Next Generation Very Large Array Memo No. 5 (<http://library.nrao.edu/ngvla.shtml>)
 Carilli, C. L. 2016, Next Generation Very Large Array Memo No. 12 (<http://library.nrao.edu/ngvla.shtml>)
 Carilli, C. L. & Shao, Y. 2017, Next Generation Very Large Array Memo No. 13 (<http://library.nrao.edu/ngvla.shtml>)
 Carilli, C. L., & Walter, F. 2013, *ARA&A*, 51, 105
 Castellano, M., Yue, B., Ferrara, A., et al. 2016, *ApJ*, 823, L40
 Chary, R.-R., & Pope, A. 2010, arXiv:1003.1731
 Chary, R. & Elbaz, D. 2010, *ApJ*, 556, 562
 Cormier, D., Madden, S. C., Leboutteiller, V., et al. 2015, *A&A*, 578, A53
 Dayal, P., Ferrara, A., Dunlop, J. S., & Pacucci, F. 2014, *MNRAS*, 445, 2545
 Dayal, Pratika, Choudhury, Tirthankar Roy, Bromm, Volker, Pacucci, Fabio 2017, *ApJ*, 836, 16
 Decarli, Roberto; Walter, Fabian; Aravena, Manuel; Carilli, Chris; Bouwens, Rychard et al. 2016, *ApJ*, 833, 69
 Decarli, R.; Walter, F.; Carilli, C.; Riechers, D.; Cox, P. et al. 2014, *ApJ*, 779, 67
 Diaz-Santos, T., Armus, L., Charmandaris, V., Lu, N., Stierwalt, S. et al. 2017, *ApJ*, in press (arXiv:1705.04326)
 De Looze, I., Cormier, D., Leboutteiller, V., et al. 2014, *A&A*, 568, A62
 Duffy, A. R., Mutch, S. J., Poole, G. B., et al. 2017, arXiv:1705.07255
 Dwek, Eli; Staguhn, Johannes; Arendt, Richard G.; Kovacks, Attila; Su, Ting; Benford, Dominic J., 2014, *ApJ*, 788, 30
 Fan, X., Carilli, C. L., & Keating, B. 2006, *ARA&A*, 44, 415
 Greig, B., & Mesinger, A. 2017, *MNRAS*, 465, 4838
 Gullberg, B., De Breuck, C., Vieira, J. D., et al. 2015, *MNRAS*, 449, 2883
 Helfer, T. T., Thornley, M. D., Regan, M. W., et al. 2003, *ApJS*, 145, 259
 Inoue, A. K., Tamura, Y., Matsuo, H., et al. 2016, *Science*, 352, 1559
 Juarez, Y., Maiolino, R., Mujinca, R., Pedani, M., Marinoni, S. et al. 2009, *A&A*, 494, L25
 Jones, G.C., Willott, C., Carilli, C. et al. 2017, *ApJ*, in press
 Laporte, N., Ellis, R. S., Boone, F., et al. 2017, arXiv:1703.02039

- Langer, W. D., Velusamy, T., Pineda, J. L., Willacy, K., & Goldsmith, P. F. 2014, *A&A*, 561, A122
- Loeb, A., & Furlanetto, S. R. 2013, *The First Galaxies in the Universe*, by Abraham Loeb and Steven R. Furlanetto. ISBN: 9780691144917. Princeton, NJ: Princeton University Press,
- Mashian, N., Oesch, P. A., & Loeb, A. 2016, *MNRAS*, 455, 2101
- Maiolino, R., Carniani, S., Fontana, A., et al. 2015, *MNRAS*, 452, 54
- Marassi, S., Schneider, R., Limongi, M., et al. 2015, *MNRAS*, 454, 4250
- McKinnon, M., Carilli, C., & Beasley, T. 2016, *Proc. SPIE*, 9906, 990627
- Michałowski, M. J., Murphy, E. J., Hjorth, J., et al. 2010, *A&A*, 522, A15
- Oesch, P. A., Brammer, G., van Dokkum, P. G., et al. 2016, *ApJ*, 819, 129
- Olsen, K., Greve, t., Narayanan, D. et al. 2017, *ApJ*, in press (arXiv:1708.04936)
- Ouchi, M., Harikane, Y., Shibuya, T., et al. 2017, arXiv:1704.07455
- Pallottini, A., Ferrara, A., Gallerani, S., et al. 2017, *MNRAS*, 465, 2540
- Parsons, A. R., Liu, A., Aguirre, J. E., et al. 2014, *ApJ*, 788, 106
- Pentericci, L., Carniani, S., Castellano, M., et al. 2016, *ApJ*, 829, L11
- Pineda, J. L., Langer, W. D., Velusamy, T., & Goldsmith, P. F. 2013, *A&A*, 554, A103
- Planck Collaboration, Adam, R., Ade, P. A. R., et al. 2016, *A&A*, 594, A1
- Riechers, D. A., Bradford, C. M., Clements, D. L., et al. 2013, *Nature*, 496, 329
- Riechers, D. A., Leung, T. K. D., Ivison, R. J., et al. 2017, arXiv:1705.09660
- Robertson, B.E., Ellis, R.S., Furlanetto, S., Dunlop, J.S. 2015, *ApJ*, 802, L19
- Selina, R. & Murphy, E. 2017, Next Generation Very Large Array Memo No. 17 (<http://library.nrao.edu/ngvla.shtml>)
- Stacey, G. J., Geis, N., Genzel, R., et al. 1991, *ApJ*, 373, 423
- Schinnerer, E., Meidt, S. E., Pety, J., et al. 2013, *ApJ*, 779, 42
- Schneider, R., Valiante, R., Ventura, P., dell'Agli, F., & di Criscienzo, M. 2015, *Why Galaxies Care about AGB Stars III: A Closer Look in Space and Time*, 497, 369
- Strandet, M. L., Weiß, A., De Breuck, C., et al. 2017, arXiv:1705.07912
- Thompson, A. R., Moran, J. M., & Swenson, G. W., Jr. 2017, *Interferometry and Synthesis in Radio Astronomy*, by A. Richard Thompson, James M. Moran, and George W. Swenson, Jr. 3rd ed. Springer, 2017.,
- Topping, M.W. & Shull, J.M. 2015, *ApJ*, 800, 97
- Vallini, L., Gallerani, S., Ferrara, A., & Baek, S. 2013, *MNRAS*, 433, 1567
- Vallini, L., Gallerani, S., Ferrara, A., Pallottini, A., & Yue, B. 2015, *ApJ*, 813, 36
- Velusamy, T., Langer, W. D., Goldsmith, P. F., & Pineda, J. L. 2015, *A&A*, 578, A135
- Venemans, B. P., Walter, F., Zschaechner, L., et al. 2016, *ApJ*, 816, 37
- Volonteri, Marta; Reines, Amy; Atek, Hakim; Stark, Daniel P.; Trebitsch, Maxime 2017, *ApJ*, submitted
- Walter, Fabian; Decarli, Roberto; Aravena, Manuel; Carilli, Chris; Bouwens, Rychard et al. 2016, *ApJ*, 833, 67
- Wang, R., Wu, X.-B., Neri, R., et al. 2016, *ApJ*, 830, 53
- Watson, D., Christensen, L., Knudsen, K. K., et al. 2015, *Nature*, 519, 327
- Wilkins, S. M., Feng, Y., Di-Matteo, T., et al. 2017, *MNRAS*, 469, 2517
- Willott, C. J., McLure, R. J., Hibon, P., et al. 2013, *AJ*, 145, 4
- Willott, C. J., Carilli, C. L., Wagg, J., & Wang, R. 2015, *ApJ*, 807, 180
- Yue, B., Ferrara, A., Pallottini, A., Gallerani, S., & Vallini, L. 2015, *MNRAS*, 450, 3829
- Yue, B., Ferrara, A., & Xu, Y. 2016, *MNRAS*, 463, 1968